Phys Chem Minerals (2012) 39:803–810
DOI 10.1007/s00269-012-0535-7

ORIGINAL PAPER

Chemistry, Raman and infrared spectroscopic characterization of the phosphate mineral reddingite: $(MnFe)_3(PO_4)_2(H_2O,OH)_3$, a mineral found in lithium-bearing pegmatite

Ray L. Frost · Yunfei Xi · Ricardo Scholz · Fernanda M. Belotti · Leonardo E. Lagoeiro

Received: 22 April 2012 / Accepted: 26 July 2012 / Published online: 18 August 2012

Abstract Detailed investigation of an intermediate member of the reddingite–phosphoferrite series, using infrared and Raman spectroscopy, scanning electron microcopy and electron microprobe analysis, has been carried out on a homogeneous sample from a lithium-bearing pegmatite named Cigana mine, near Conselheiro Pena, Minas Gerais, Brazil. The determined formula is $(Mn_{1.60}Fe_{1.21}Ca_{0.01}Mg_{0.01})_{\sum 2.83}(PO_4)_{2.12} \cdot (H_2O_{2.85}F_{0.01})_{\sum 2.86}$, indicating predominance in the reddingite member. Raman spectroscopy coupled with infrared spectroscopy supports the concept of phosphate, hydrogen phosphate and dihydrogen phosphate units in the structure of reddingite-phosphoferrite. Infrared and Raman bands attributed to water and hydroxyl stretching modes are identified. Vibrational spectroscopy adds useful information to the molecular structure of reddingite–phosphoferrite.

Keywords Raman · Infrared · Molecular structure · Reddingite–phosphoferrite · Phosphate · Pegmatite

Introduction

Reddingite is an uncommon manganese hydrated phosphate mineral with general chemical formula expressed as $(MnFe)_3(PO_4)_2(H_2O,OH)_3$ and belongs to the phosphoferrite group. In general, members have the formula $(M1)(M2)_2(PO_4)_2(H_2O,OH)_3$. The mineral forms a complex triple series with phosphoferrite, its Fe^{2+} analogue and with kryzhanovskite, the Fe^{3+} analogue (Moore et al. 1980). Other minerals related to the group are landesite and garyansellite.

According to Tennyson (1954), reddingite crystallizes in orthorhombic symmetry of *Pmna* space group with unit-cell parameters $a = 9.49$ Å, $b = 10.08$ Å, $c = 8.07$ Å and $V = 832.24$ Å^3. It is a common mineral in lithium-bearing pegmatites and is related to the hydrothermal alteration after triphylite–lithiophilite (Roda et al. 2004). Moore (1973) described phosphoferrite as a late hydrothermal mineral in the phosphate paragenesis of pegmatites. Nriagu and Dell (1974) carried out thermochemical studies for low-temperature basic iron phosphates and suggest the formation of phosphoferrite–reddingite solid solution in phosphorus-rich sediments, during the diagenetic process, in reducing environments. The crystallization of authigenic minerals in sediments develops an important function in the removal and storage of heavy metals and phosphate pollutants.

The crystal structures of phosphoferrite and kryzhanovskite were detemined by Moore and Araki (1976), and the similarities between the two crystal structures can be applied to the crystal structure of reddingite. The structure is based on sheets of corner- and edge-linked octahedra that are oriented parallel to {100}. The phosphate tetrahedra are situated

Electronic supplementary material The online version of this article (doi:10.1007/s00269-012-0535-7) contains supplementary material, which is available to authorized users.

R. L. Frost (✉) · Y. Xi
Science and Engineering Faculty, School of Chemistry, Physics and Mechanical Engineering, Queensland University of Technology, GPO Box 2434, Brisbane, QLD 4001, Australia
e-mail: r.frost@qut.edu.au

R. Scholz · L. E. Lagoeiro
Geology Department, School of Mines, Federal University of Ouro Preto, Campus Morro do Cruzeiro, Ouro Preto, MG 35400-00, Brazil

F. M. Belotti
Federal University of Itajubá, Campus Itabira, Itabira, MG 35903-087, Brazil

between these symmetry-equivalent octahedral sheets and link by corner sharing. As a result, the structure is a rather rigid framework of octahedra and tetrahedra and the crystals exhibit no good cleavage.

As suggested by Moore and Araki (1976), the mechanism of oxidation of Fe^{2+} to Fe^{3+} in the phosphoferrite–kryzhanovskite series can be expressed as $2Fe^{2+}(H_2O) \rightarrow 2Fe^{3+}(OH)^- + H_2$. The presence of OH^- anion is indicative of Fe^{3+} in the structure. Studies concerning the mineralogy of phosphoferrite group minerals are rare in the literature (Sturman and Dunn 1984; Dill et al. 2009), and data about spectroscopic characterization are restricted to the database of the University of Arizona (rruff.info); however, no interpretation is given. In the study of similar phases, infrared spectroscopic characterization of manganese phosphate pentahydrate calcined at 400 °C was carried out by Sarawadekar and Kulkarni (1983), who also described the dehydration at temperatures up to 405 °C. No Raman spectroscopic investigation of these phosphate phases related to the phosphoferrite group has been published. However, in recent years, the application of spectroscopy to understand the structure of phosphates has been on the increase (Dias et al. 2011; Frost and Xi 2012).

S. D. Ross in Farmer's treatise (1974) divided the vibrational spectra of phosphates according to the presence or absence of water and/or hydroxyl units. In aqueous systems, the Raman spectra of phosphate oxyanions show a symmetric stretching mode (v_1) at 938 cm^{-1}, the antisymmetric stretching mode (v_3) at 1,017 cm^{-1}, the symmetric bending mode (v_2) at 420 cm^{-1} and the v_4 out-of-plane bending mode at 567 cm^{-1}. The value for the v_1 symmetric stretching vibration of PO_4 units as determined by infrared spectroscopy was also described (Frost et al. 2002a, b, c). The position of the symmetric stretching vibration is mineral dependent and a function of the cation and crystal structure. The fact that the symmetric stretching mode is observed in the infrared spectrum affirms a reduction in symmetry of the PO_4 units.

The value for the v_2 symmetric bending vibration of PO_4 units as determined by infrared spectroscopy was given as 438 cm^{-1} (augelite), 452 cm^{-1} (wavellite), 440 and 415 cm^{-1} (rockbridgeite), 455, 435 and 415 cm^{-1} (dufrenite) and 470 and 450 cm^{-1} (beraunite). The observation of multiple bending modes provides an indication of symmetry reduction of the PO_4 units. This symmetry reduction is also observed through the v_3 antisymmetric stretching vibrations. Augelite shows infrared bands at 1,205, 1,155, 1,079 and 1,015 cm^{-1} (Frost and Weier 2004); wavellite at 1,145, 1,102, 1,062 and 1,025 cm^{-1}; rockbridgeite at 1,145, 1,060 and 1,030 cm^{-1}; dufrenite at 1,135, 1,070 and 1,032 cm^{-1}; and beraunite at 1,150, 1,100, 1,076 and 1,035 cm^{-1}.

In the infrared study of triploidite, a basic manganese phosphate, Farmer reports the infrared spectrum with the (v_1) at 957 cm^{-1}, (v_3) at 1,090, 1,058, 1,030 and 1,010 cm^{-1}, (v_2) at 420 cm^{-1} and the v_4 mode at 595, 570 and 486 cm^{-1} (Frost and Xi 2012). A hydroxyl stretching wavenumber of 3,509 cm^{-1} was tabled. In the infrared spectroscopic study of strengite, in the region below 400 cm^{-1}, Frost and Weier (2004) described the metal stretching vibrations for MnO and the OMnO bending modes.

In this work, samples of a pure, monomineral reddingite from the Cigana pegmatite, located in the municipality of Conselheiro Pena, Brazil, have been carried out. Studies include chemistry with analysis via electron microprobe (EMP) in the WDS mode and the spectroscopic characterization of the structure with infrared and Raman.

Experimental

Samples description and preparation

The reddingite samples were collected from the Cigana mine (also named João Claim), a lithium-bearing pegmatite located in the Conselheiro Pena Pegmatite district (CPD), one of the eleven metallogenetic subdivisions of the Eastern Brazilian Pegmatite Province (EBP) in Minas Gerais (Pedrosa-Soares et al. 2011). Geological description of the CPD and the complete paragenesis of the Cigana pegmatite have been described by Chaves et al. (2005).

In the Cigana mine, brown reddish reddingite crystals up to 4.0 mm along the **c** axis with octahedral morphology occur in association with vivianite, lithiophilite and hureaulite. The sample came from the collection of the Geology Department of the Federal University of Ouro Preto, Minas Gerais, Brazil, with sample code SAA-081. The reddingite crystals were hand selected. The sample was gently crushed and the associated minerals were removed under a stereomicroscope Leica MZ4. The reddingite crystals were phase analyzed by X-ray diffraction. Scanning electron microscopy (SEM) was applied to support the chemical characterization and indicate the elements to be analyzed by EMP. Thermogravimetric analysis was undertaken to support the H_2O determination.

X-ray diffraction (XRD)

Powder X-ray diffractograms (XRD) were obtained with a PANalytical Empyrean diffractrometer equipped with a Cu tube and a nickel filter with the facilities of the Geology Department of the Federal University of Ouro Preto. The scanning was done at 25 °C from 4° to 70° (2θ) at 0.25° per minute with an X-ray accelerator, using silicon as external standard. Cell parameters were calculated by Rietveld

refinement using intensity and angular weighting of the most intense peaks.

Thermogravimetric analysis: TG/DTG

Thermogravimetric analysis of the reddingite mineral was obtained by using TA Instruments Inc. Q500 high-resolution TGA operating at a 5 °C/min ramp with 6.0 °C resolution from room temperature to 1,000 °C in a high-purity flowing nitrogen atmosphere (40 cm^3/min). Approximately 65 mg of finely ground dried sample was heated in an open platinum crucible.

Electron microprobe analysis (EMP)

EMP was performed in a reddingite single crystal. The chemical analysis was done on a Jeol JXA8900R with four WDS spectrometers at the Physics Department of the Federal University of Minas Gerais, Belo Horizonte. For each selected element, the following standards were applied: Mn (rhodonite), Fe (magnetite), Ca ($Ca_2P_2O_7$), Mg (MgO), F (fluorite) and P ($Ca_2P_2O_7$). Samples of reddingite embedded in an epoxy resin were coated with a thin layer of evaporated carbon. The EMPA was performed at 15 kV of accelerating voltage and beam current of 10 nA.

Raman microprobe spectroscopy

Crystals of reddingite were placed on a polished metal surface on the stage of an Olympus BHSM microscope, which is equipped with 10×, 20× and 50× objectives. The microscope is part of a Renishaw 1,000 Raman microscope system, which also includes a monochromator, a filter system and a CCD detector (1,024 pixels). The Raman spectra were obtained using a Spectra-Physics model 127 He–Ne laser producing highly polarized light at 633 nm and collected at a nominal resolution of 2 cm^{-1} and a precision of ±1 cm^{-1} in the range between 200 and 4,000 cm^{-1}. Repeated acquisitions on the crystals using the highest magnification (50×) were accumulated to improve the signal-to-noise ratio of the Raman spectra. Raman Spectra were calibrated using the 520.5 cm^{-1} line of a silicon wafer. The Raman spectrum of at least 10 crystals was collected to ensure the consistency of the spectra.

Infrared spectroscopy

Infrared spectra were obtained using a Nicolet Nexus 870 FTIR spectrometer with a smart endurance single-bounce diamond ATR cell. Spectra over the 4,000–525 cm^{-1} range were obtained by the co-addition of 128 scans with a resolution of 4 cm^{-1} and a mirror velocity of 0.6329 cm/s. Spectra were co-added to improve the signal-to-noise ratio. The infrared spectra are given in the supplementary information.

Spectral manipulation such as baseline correction/adjustment and smoothing was performed using the Spectracalc software package GRAMS (Galactic Industries Corporation, NH, USA). Band component analysis was undertaken using the Jandel "Peakfit" software package that enabled the type of fitting function to be selected and allows specific parameters to be fixed or varied accordingly. Band fitting was done using a Lorentzian-Gaussian cross-product function with the minimum number of component bands used for the fitting process. The Gaussian–Lorentzian ratio was maintained at values greater than 0.7 and fitting was undertaken until reproducible results were obtained with squared correlations of r^2 greater than 0.995.

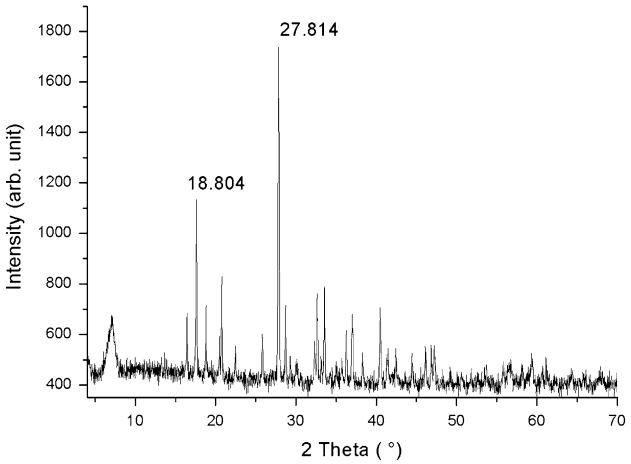

Fig. 1 X-ray diffraction pattern of reddingite at 25 °C. The two most intense peaks are shown

Table 1 Chemical composition of reddingite-phosphoferrite from Cigana pegmatite (mean of 4 electron microprobe analyses)

Constituent	wt.%	Number of cations	Range (wt.%)	Probe standard
MnO	28.44	1.60	27.10–29.82	Rhodonite
FeO	21.87	1.21	19.44–24.44	Magnetite
CaO	0.10	0.01	0.02–0.22	$Ca_2P_2O_7$
MgO	0.06	0.01	0.02–0.18	MgO
P_2O_5	37.70	2.12	36.17–38.39	$Ca_2P_2O_7$
H_2O	12.91	2.85	Calculated by loss of mass (TG)	
F	0.06	0.01	0.00–0.19	Fluorite
O–F	−0.03			
Total	101.17			

H_2O calculated by thermogravimetric analysis

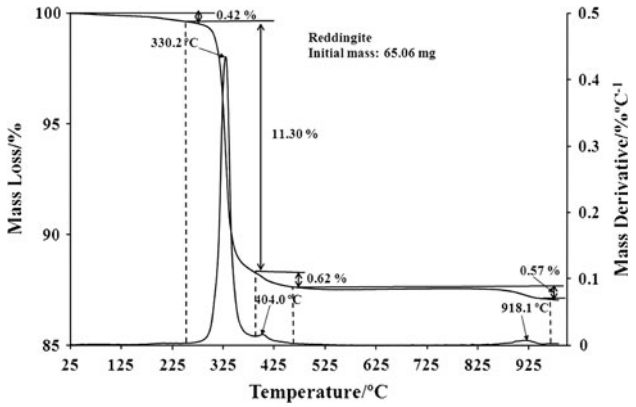

Fig. 2 TG/DTG pattern of reddingite

Results and discussion

Mineralogical and chemical characterization

The mineral phase reddingite was identified by XRD, and the diffractogram is shown in the Fig. 1. The unit-cell parameters were calculated by Rietveld refinement and are given as: $a = 9.4889$ (7), $b = 10.1260$ (7) and $c = 8.7102$ (6) Å. The calculated values are in agreement with the phosphoferrite group and the published data for reddingite (Tennyson 1954).

The quantitative chemical analysis of reddingite is presented in Table 1. Composition is the result of the average of four spots. H_2O content was measured by mass loss (ML) observed in the TG curve (Fig. 2), where $ML = H_2O + F$. The chemical formula was calculated on the basis of 11 oxygen atoms (O, H_2O, F) in the structure. The spectroscopic characterization carried out in this work indicates the presence of H_2O in the structure and the absence of OH^-. The TG curve of reddingite shows a total mass loss of 12.91 % on heating to 950 °C in nitrogen flux.

The chemical composition indicates an intermediate member of the reddingite-phosphoferrite series with predominance of reddingite in relation to the phosphoferrite end member. The chemical analysis shows 28.44 % of MnO and 21.87 % of FeO. Traces of Ca and Mg were also found (0.10 % CaO and 0.06 % MgO). Due to the absence of OH^- in the structure as supported by infrared and Raman spectroscopy, the total iron content is considered as Fe^{2+}, as shown in the chemical formula:

$$(Mn_{1.60}Fe_{1.21}Ca_{0.01}Mg_{0.01})_{\sum 2.83}(PO_4)_{2.12} \cdot (H_2O_{2.85}F_{0.01})_{\sum 2.86}$$

Spectroscopy

The Raman spectrum over the 100–4,000 cm^{-1} spectral range is displayed in Fig. 3a. This figure shows the relative intensity and position of the various bands. There are parts of the spectrum where no intensity is observed. Therefore, the spectrum is subdivided into sections depending upon the types of vibration being studied. The infrared spectrum of reddingite is reported in Fig. 3b. In a similar fashion, the IR spectrum is divided into sections for further detailed analysis. The Raman spectrum of reddingite in the

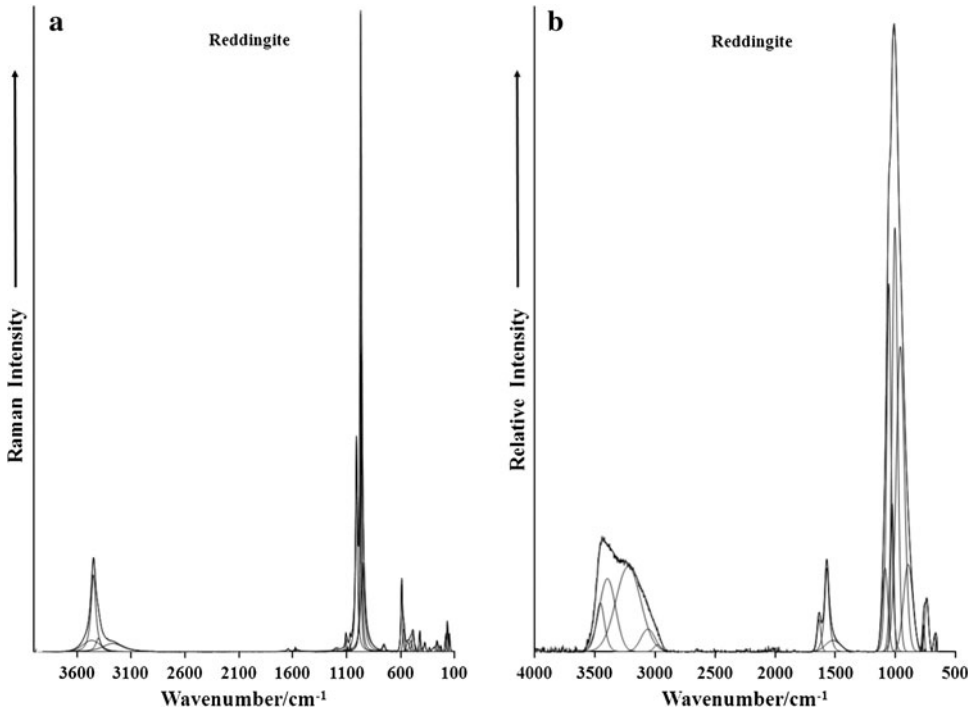

Fig. 3 **a** Raman spectrum of reddingite in the 100–4,000 cm^{-1} spectral range, **b** infrared spectrum of reddingite in the 500–4,000 cm^{-1} spectral range

800–1,400 cm^{-1} spectral range is shown in Fig. 4a. The spectrum is dominated by a sharp band at 970 cm^{-1}, which may be deconvoluted into component bands at 951, 963 and 970 cm^{-1}. This band is attributed to the symmetric PO_4^{3-} stretching vibration. A second strong Raman band at 1,007 cm^{-1} is attributed to symmetric $HOPO_3^{2-}$ stretching vibration. The series of low-intensity Raman bands at 1,064, 1,093, 1,104 and 1,193 cm^{-1} are assigned to the PO_4^{3-} and $HOPO_3^{2-}$ antisymmetric stretching vibrations. In the infrared spectrum (Fig. 4b), a broad spectral profile is observed with curve-resolved band components delineated at 959, 1,004, 1,026, 1,054 and 1,086 cm^{-1}. These

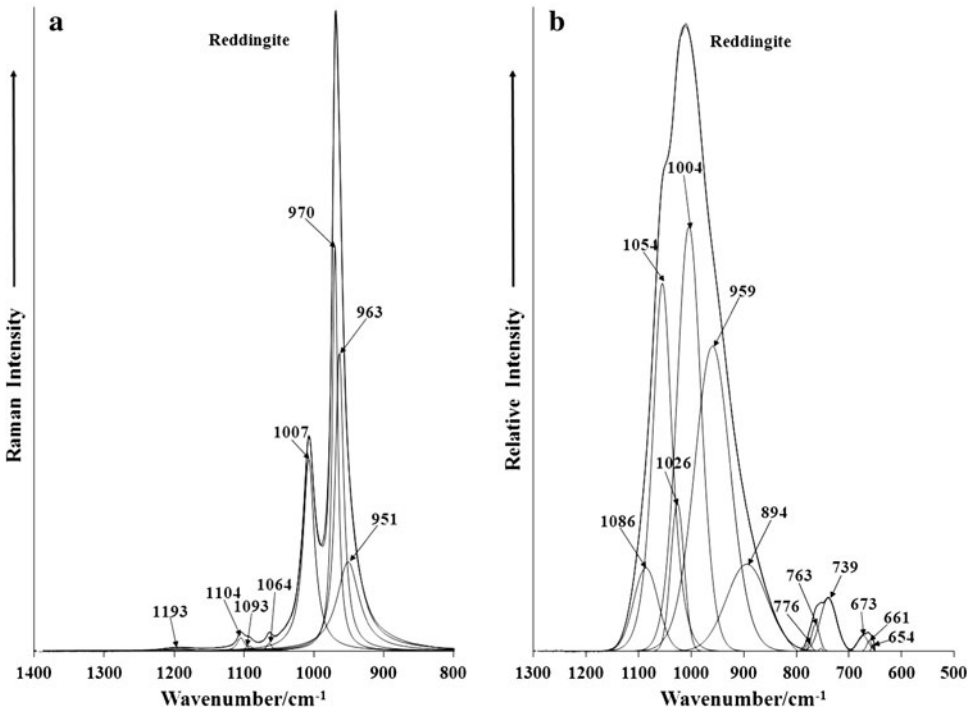

Fig. 4 **a** Raman spectrum of reddingite in the 800–1,400 cm^{-1} spectral range, **b** infrared spectrum of reddingite in the 500–1,300 cm^{-1} spectral range

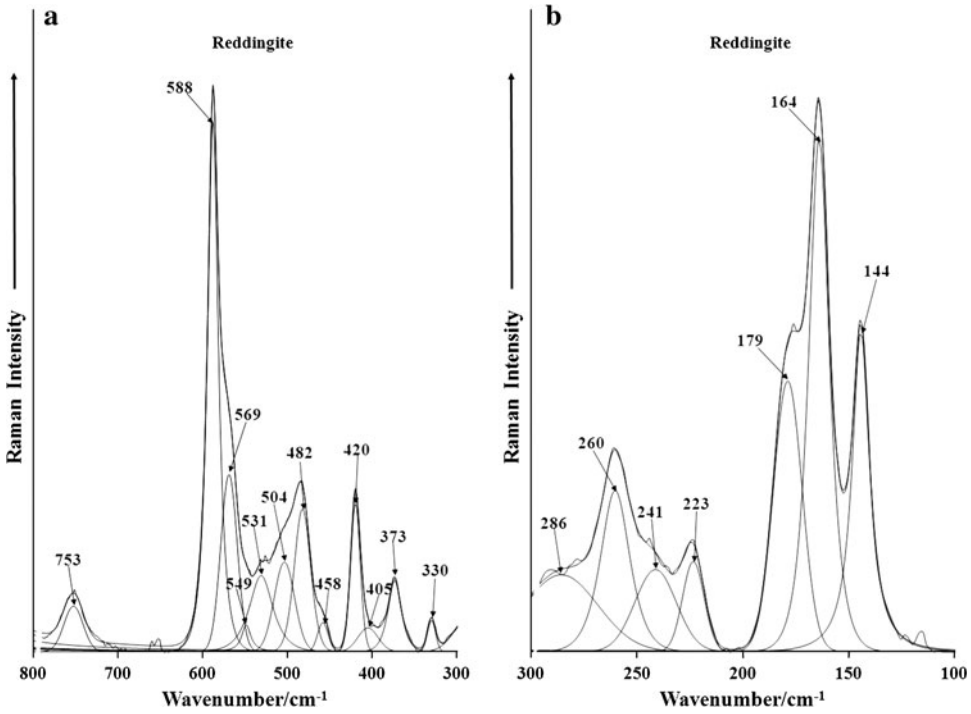

Fig. 5 **a** Raman spectrum of reddingite in the 300–800 cm^{-1} spectral range, **b** Raman spectrum of reddingite in the 100–300 cm^{-1} spectral range

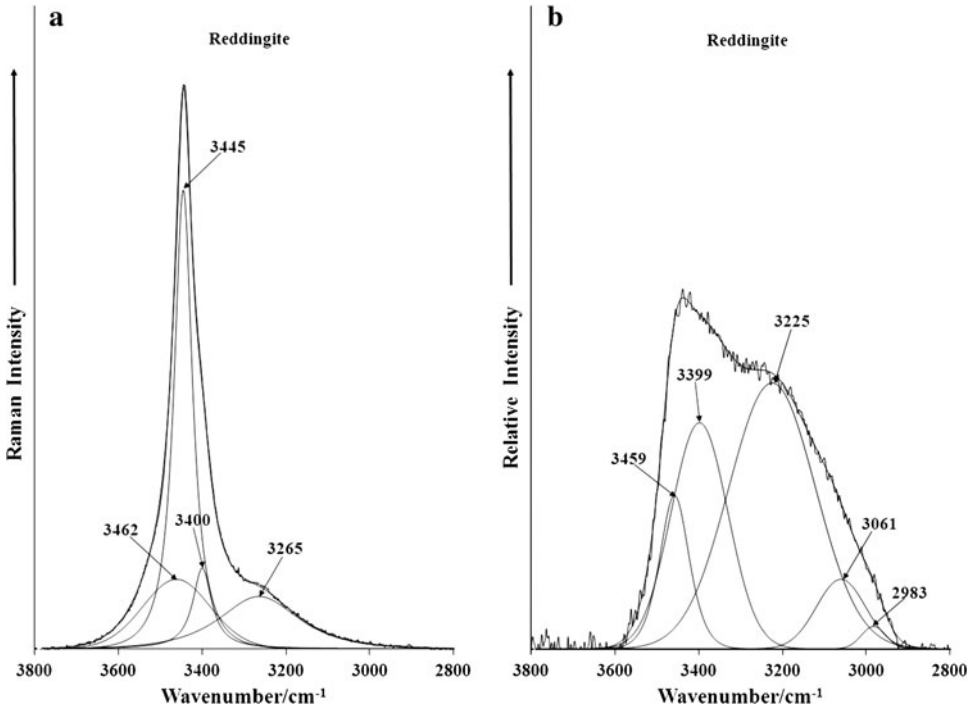

Fig. 6 **a** Raman spectrum of reddingite in the 2,800–3,800 cm^{-1} spectral range, **b** infrared spectrum of reddingite in the 2,800–3,800 cm^{-1} spectral range

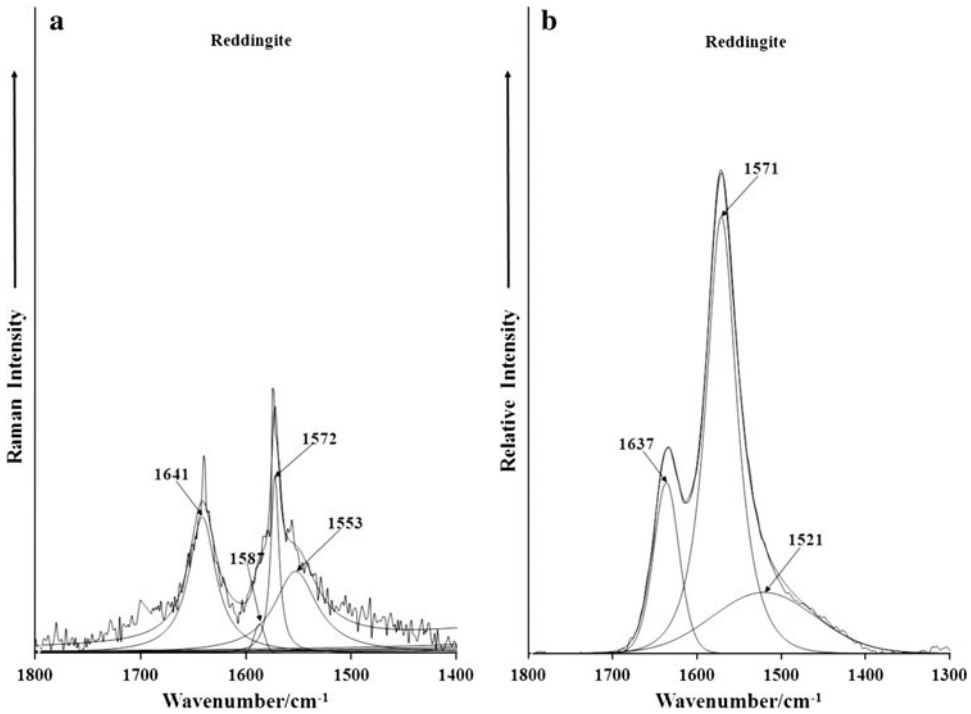

Fig. 7 **a** Raman spectrum of reddingite in the 1,400–1,800 cm^{-1} spectral range, **b** infrared spectrum of reddingite in the 1,300–1,800 cm^{-1} spectral range

bands are a combination of the PO_4^{3-} and $HOPO_3^{2-}$ antisymmetric and symmetric stretching vibrations. The low-intensity infrared bands centered upon 673 and 739 cm^{-1} are thought to be due to water librational modes. The observation of multiple bands supports the concept that not all the water molecules in the structure of reddingite are equivalent.

The Raman spectrum of reddingite in the 300–800 cm^{-1} spectral range and in the 100–300 cm^{-1} spectral range is reported in Fig. 5a, b. An intense Raman band at 588 cm^{-1}

with shoulders at 549 and 569 cm^{-1} is assigned to the v_4 out-of-plane bending modes of the PO_4 and $HOPO_3$ units. The series of bands at 420, 458, 482, 504 and 531 cm^{-1} are attributed to the v_2 PO_4 and $HOPO_3$ bending modes. The low-intensity Raman bands at 330 and 373 cm^{-1} are attributed to metal–oxygen stretching vibrations. In the far low wavenumber region, strong Raman bands are found at 144, 164 and 179 cm^{-1} with bands of lower intensity at 223, 241, 260 and 286 cm^{-1}. These bands are due to external vibrations and may simply be described as lattice vibrations.

The Raman spectrum of reddingite in the OH stretching region is illustrated in Fig. 6a, while the infrared spectrum in the 2,800–3,800 cm^{-1} spectral range is reported in Fig. 6b. The Raman spectrum of reddingite displays a very intense band at 3,445 cm^{-1} with a shoulder at 3,265 cm^{-1} and is assigned to water stretching vibrations. In contrast, the infrared spectrum shows a series of overlapping bands in quite a broad spectral profile. Infrared bands are observed at 3,061, 3,225, 3,399 and 3,459 cm^{-1}. These bands are assigned to a combination of water antisymmetric and symmetric stretching modes. The position of the bands in both the Raman and infrared spectra supports the concept that the water molecules are involved in quite strong hydrogen bonding in the structure of reddingite. This concept is supported by the observation of water bending modes observed at 1,641 cm^{-1} in the Raman spectrum and 1,637 cm^{-1} in the infrared spectrum (Fig. 7a, b). These bands are due to the bending modes of quite strongly hydrogen-bonded water. In non-hydrogen-bonded water as may be found in water vapor, the band occurs at 1,595 cm^{-1}. In weakly hydrogen-bonded systems, the band occurs at 1,620 cm^{-1}.

Conclusions

An intermediate member of the reddingite-phosphoferrite series was studied by Raman and infrared spectroscopy. The chemical characterization was carried out by EMP and shows chemical formula expressed by $(Mn_{1.60}Fe_{1.21}Ca_{0.01}Mg_{0.01})_{\sum 2.83}(PO_4)_{2.12}(H_2O_{2.85}F_{0.01})_{\sum 2.86}$, that indicate predominance in the reddingite member.

The spectroscopic study indicates the presence of H_2O and the absence of OH^- in the structure. Raman assigned bands to water stretching vibrations were observed in the region of 3,445 cm^{-1} and 3,265 cm^{-1}. The infrared spectrum shows a series of overlapping bands at 3,061, 3,225, 3,399 and 3,459 cm^{-1} assigned to a combination of water antisymmetric and symmetric stretching modes. The absence of OH^- suggests the presence of Fe^{2+}. Vibrational spectroscopy enables new knowledge of the structure of reddingite to be understood.

Acknowledgments The financial and infrastructure support of the Discipline of Nanotechnology and Molecular Science, Science and Engineering Faculty of the Queensland University of Technology is gratefully acknowledged. The Australian Research Council (ARC) is thanked for funding the instrumentation. We also gratefully acknowledge the contributions of the Fundação de Amparo à Pesquisa do Estado de Minas Gerais—FAPEMIG—grant No. CRA—APQ-03998-10.

References

Chaves MLSC, Scholz R, Atencio D, Karfunkel J (2005) Assembléias e paragêneses minerais singulares nos pegmatitos da região de Galiléia (Minas Gerais). Geociências 24:14–161 (in Portuguese)

Dias LN, Pinheiro MVB, Moreira RL, Krambrock K, Guedes K, Menezes Filho LAD, Karfunkel J, Schnellrath J, Scholz R (2011) Spectroscopic characterization of transition metal impurities in natural montebrasite/amblygonite. Am Min 96:42–52

Dill HG, Weber B, Gerdes A, Melcher F (2009) The Fe-Mn phosphate aplite 'Silbergrube' near Waidhaus, Germany: epithermal phosphate mineralization in the Hagendorf-Pleystein pegmatite province. Min Mag 7:1119–1144

Farmer VC (1974) Mineralogical society monograph 4: the infrared spectra of minerals. The Mineralogical Society, London, p 427

Frost RL, Weier ML (2004) Vibrational spectroscopy of natural augelite. J Mol Struc 697:207–211

Frost RL, Xi Y (2012) Molecular structure of the phosphate mineral brazilianite $NaAl_3(PO_4)_2(OH)_4$: a semi precious jewel. J Mol Struc 1010:179–183

Frost RL, Martens W, Williams PA, Kloprogge JT (2002a) Raman and infrared spectroscopic study of the vivianite-group phosphates vivianite, baricite, and bobierrite. Min Mag 66:1063–1073

Frost RL, Martens WN, Kloprogge T, Williams PA (2002b) Vibrational spectroscopy of the basic manganese, ferric and ferrous phosphate minerals: strunzite, ferristrunzite and ferrostrunzite. Neues Jb Miner Monat 11:481–496

Frost RL, Williams PA, Martens W, Kloprogge JT, Leverett P (2002c) Raman spectroscopy of the basic copper phosphate minerals cornetite, libethenite, pseudomalachite, reichenbachite and ludjibaite. J Raman Spectrosc 33:260–263

Moore PB (1973) Pegmatite phosphates: descriptive mineralogy and crystal chemistry. Min Rec 4:103–130

Moore PB, Araki T (1976) A mixed-valence solid-solution series: crystal structure of phosphoferrite $(Fe^{2+})_3(H_2O)_3[PO_4]_2$. Inorg Chem 15:316–321

Moore PB, Araki T, Kampf AR (1980) Nomenclature of the phosphoferrite structure type: refinements of landsite and kryzhanovskite. Min Mag 43:789–795

Nriagu JO, Dell CI (1974) Diagenetic formation of iron phosphates in recent lake sediments. Arner Min 59:934–946

Pedrosa-Soares AC, de Campos CM, Noce CM, da Silva LC, Novo TA, Roncato J, Medeiros SM, Castañeda C, Queiroga GN, Dantas E, Dussin IA, Alkmim F (2011) Late Neoproterozoic-Cambrian granitic magmatism in Araçuaí orogen (Brazil), the Eastern Brazilian Pegmatite Province and related mineral resources. Geol Soc Spec Pub 350:25–51

Roda E, Pesquera A, Fontan F, Keller P (2004) Phosphate mineral associations in the Cañada pegmatite (Salamanca, Spain):

paragenetic relationships, chemical compositions, and implications for pegmatite evolution. Am Min 89:110–125
Sarawadekar RG, Kulkarni SB (1983) Physico-chemical properties of metal phosphates. Thermochim Acta 67:341–349
Sturman BD, Dunn PJ (1984) Garyansellite, a new mineral from Yukon Territory, Canada. Am Min 69:207–209
Tennyson C (1954) Phosphoferrit und reddingit von Hagendorf. Neues Jb Miner Monat Ab 87:185–217